ACS OMEGA

http://pubs.acs.org/journal/acsodf

Article

Structural Defects and Ferromagnetic Signature of V-Doped Sb_2Te_3 Thin Films Grown on $SrTiO_3(001)$ Produced by RF-Magnetron Sputtering

Kazuhisa Sato*

Cite This: *ACS Omega* 2022, 7, 40480−40484

Read Online

ACCESS | Metrics & More | Article Recommendations | Supporting Information

ABSTRACT: Thin films of V-doped Sb_2Te_3 compounds were fabricated by co-deposition of Sb_2Te_3 and V using rf-magnetron sputtering onto $SrTiO_3(001)$ substrates kept at 570 K. The microstructures of the films were characterized using transmission electron microscopy (TEM) and electron diffraction. The crystal structure of the sputtered film ($Sb_{38}V_2Te_{60}$) is the Bi_2Te_3-type structure with lattice parameters of a = 0.44 ± 0.03 nm and c = 3.02 ± 0.02 nm. A combination of cross-sectional and plan-view TEM observations revealed the preferential orientation of the c axis in the film's normal direction. A thin amorphous layer exists between the Sb_2Te_3 thin film and the $SrTiO_3$ substrate. The interfacial amorphous layer relaxes the strain between the thin film and the substrate, and hence, it should promote the growth of a low-index atomic plane with a low surface free energy (i.e., (0001) of the Sb_2Te_3). The onset of ferromagnetic order was detected at temperatures below 70 K. A remarkable increase in magnetization was detected in the film's normal direction, which corresponds to the magnetic easy axis (i.e., c axis of the Sb_2Te_3). V^{3+} ions substituting Sb sites should contribute to ferromagnetism at low temperatures.

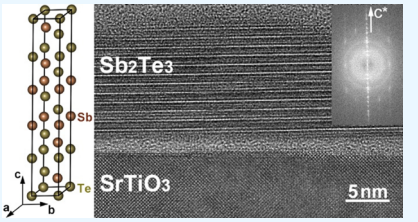

INTRODUCTION

A p-type thermoelectric semiconductor, Sb_2Te_3, is also known to be a topological insulator (TI)[1,2] and exhibits quantum anomalous Hall effects when V, Cr, or Bi is added.[3−5] Atomically controlled thin film structures are the key to manifesting the physical properties of TIs, and hence, molecular beam epitaxy (MBE) in an ultrahigh vacuum has been used for epitaxial growth of TI thin films.[3−7] In contrast, mass synthesis of TI thin films in a low vacuum is desired from an application point of view. We have studied the fabrication of chalcogenide compound thin films using the sputtering method.[8] The magnetron sputtering technique enables high-speed deposition (1−10 nm/s), which is more than three times faster than the MBE, in an inert gas atmosphere (1−100 mTorr), and is expected to be a novel deposition process for Sb_2Te_3 thin films.

Sb_2Te_3 is a line compound with a trigonal Bi_2Te_3-type structure (space group: $R\bar{3}m$, a = 0.4264 nm, and c = 3.0458 nm).[9,10] The crystal structure is shown in Figure S1 in the Supporting Information. The structure is composed of a structural unit "Te−Sb−Te−Sb−Te" connected by ionic and covalent bonds.[11] Te−Te bonding between the adjacent quintuple layers is due to the van der Waals (vdW) force. Namely, the structural units are loosely connected in the [0001] direction (c axis) by the vdW force to form an anisotropic crystal structure. The c axis corresponds to the magnetic easy axis of the V-doped Sb_2Te_3 single crystals that act as diluted magnetic semiconductors.[11] Therefore, orientation control of the c axis is the most important factor for controlling the magnetic properties of V-doped Sb_2Te_3.

In this study, we have studied crystal orientation, microstructure, and structural defects of the sputtered V-doped Sb_2Te_3 thin films using transmission electron microscopy (TEM) and electron diffraction. An aligned c axis was realized, and a ferromagnetic signature was detected for the sputter-deposited thin films. We show that rf-magnetron sputtering is a new route to produce V-doped Sb_2Te_3 thin films with a well-defined film structure.

RESULTS AND DISCUSSION

Cross-Sectional TEM Observation. Figure 1a shows a bright-field TEM image of a cross section of a V-doped Sb_2Te_3 thin film sputtered for 60 s. A flat island-like morphology is seen on the $SrTiO_3(001)$ substrate. The Sb_2Te_3 islands were in contact with each other and formed a continuous film. The V content was determined to be ≈2 at % by TEM−EDS analysis ($Sb_{38}V_2Te_{60}$, see Figure S2). Figure 1b shows a selected area electron diffraction (SAED) pattern of the specimen shown in Figure 1a. Strong diffraction spots are due to the $SrTiO_3$ substrate with [010] beam incidence. Weak streaks exist in the [001]* direction across the fundamental reflections of the

Received: August 31, 2022
Accepted: October 21, 2022
Published: October 31, 2022

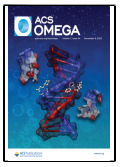

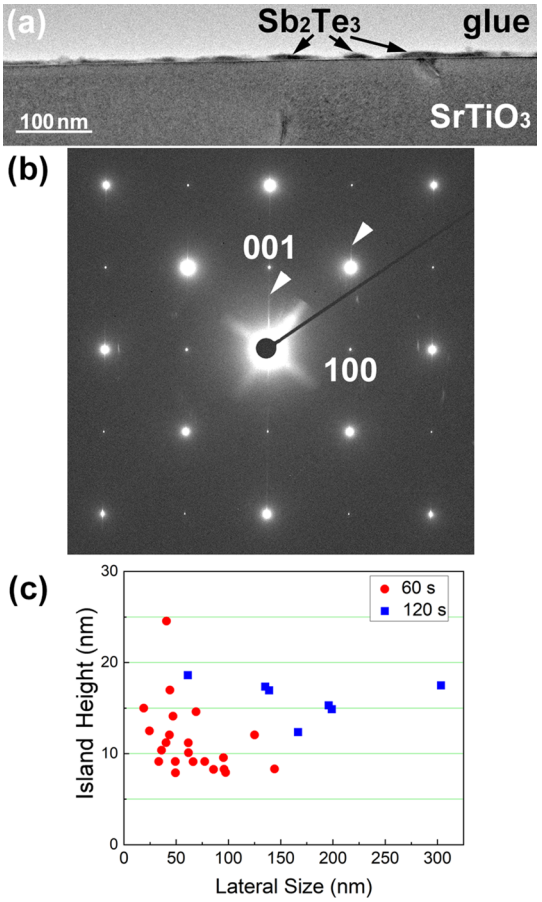

Figure 1. (a) Cross-sectional TEM image of the V-doped Sb_2Te_3 thin film sputtered for 60 s. (b) SAED pattern. (c) Relationship between island height and lateral island size for films sputtered at 60 s (solid circles) and 120 s (solid squares).

$SrTiO_3$ as indicated by arrowheads. These streaks are due to the thin Sb_2Te_3 plate grown on the substrate surface. Figure 1c shows the relationship between island height and lateral island size for films sputtered at 60 s (solid circles) and 120 s (solid squares). As the sputtering duration increases, the lateral size markedly increases compared with the island height. A noticeable feature is that the island height is almost independent of the lateral island size. This result indicates that Sb_2Te_3 grows faster in the lateral direction during the crystal growth on the $SrTiO_3$(001) substrate. The surface free energy of Sb_2Te_3 (0.03−0.07 J/m^2)[12] is much lower than that of the $SrTiO_3$ (1.09 J/m^2),[13] also justifying the lateral growth of Sb_2Te_3 on the $SrTiO_3$ substrate.

Figure 2a shows a cross-sectional high-resolution TEM (HREM) image of the V-doped Sb_2Te_3 thin film sputtered for 60 s. The beam incidence is in the [010]$SrTiO_3$ direction. Fast Fourier transforms (FFTs) of the Sb_2Te_3 film obtained from the area enclosed by rectangular frames are shown in Figure 2b−d. The FFT pattern shown in Figure 2b can be indexed by the $[10\bar{1}0]$ incidence of the trigonal Bi_2Te_3-type structure. The *c* axis is oriented out-of-plane and slightly tilted (≈1.5°) from the direction perpendicular to the film surface. This can be confirmed by the inclination of the 000*l* ($l = 3n$) systematic reflections of the FFT patterns as well as tilted periodic lattice fringes in the HREM image with respect to the $SrTiO_3$ substrate. In contrast to the out-of-plane direction with aligned *c* axis orientation, the crystal is rotated in the film plane as

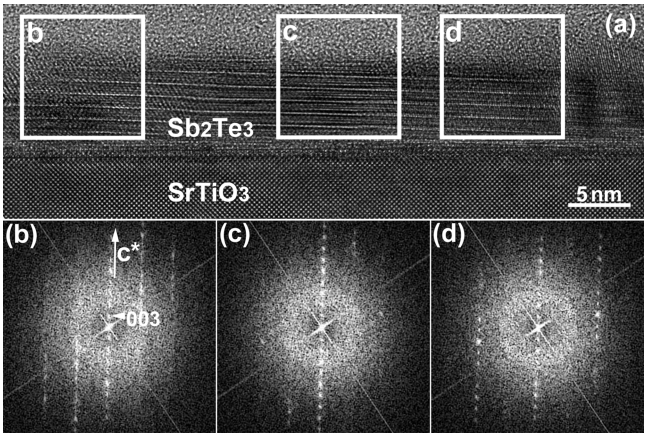

Figure 2. (a) Cross-sectional HREM image of the V-doped Sb_2Te_3 thin film sputtered for 60 s. FFT patterns (b), (c), and (d) were obtained from the area enclosed by rectangular frames marked as b, c, and d, respectively.

demonstrated by the deviation of FFT patterns shown in Figure 2c,d from the zone axis.

Figure 3a shows a cross-sectional HREM image of the V-doped Sb_2Te_3 thin film sputtered for 120 s. As seen, there exists a

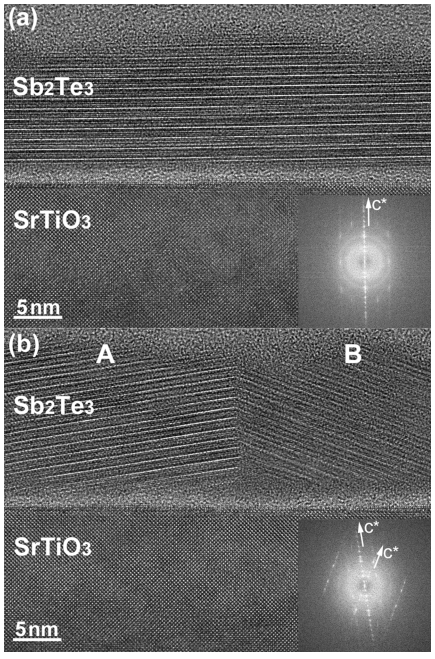

Figure 3. Cross-sectional HREM images of the V-doped Sb_2Te_3 thin film sputtered for 120 s. (a) Single crystal region. (b) Region including a grain boundary. The FFT patterns were obtained from the central part of the Sb_2Te_3 films shown in each image.

thin amorphous layer between the Sb_2Te_3 and the $SrTiO_3$ substrate. The thickness of the amorphous layer is in the range of approximately 1.2−1.9 nm. STEM−EDS analysis revealed that the amorphous layer is composed of Sb_2Te_3 (Figures S3 and S4). In both the crystalline and the amorphous layers, the ratio of Sb to Te was approximately 2:3, and no significant difference was observed. We also confirmed the surface crystallinity of the substrate using reflection high-energy electron diffraction (Figure S5): sharp diffraction patterns were obtained before and after annealing at 570 K (film growth temperature).

https://doi.org/10.1021/acsomega.2c05634
ACS Omega 2022, 7, 40480−40484

Therefore, it is concluded that the observed amorphous layer is composed of Sb_2Te_3 instead of $SrTiO_3$. A similar amorphous-like contrast can be seen on an image of the $Sb_{2-x}V_xTe_3$ film grown on the Si(111) substrate reported by Li et al.[4] This means that an amorphous layer may be formed independently of the substrate material. It is presumed that the amorphous layer is formed to relax the lattice strain between the single-crystal substrate and the Sb_2Te_3 film. Once the strain is relaxed, the (0001) atomic plane, which is a low-index atomic plane with low surface free energy,[12] preferentially grows on the amorphous layer, and hence, the *c* axis tends to orient perpendicular to the film plane. The FFT pattern shown in Figure 3a was obtained from the Sb_2Te_3 film. The tilt of the *c* axis is about 0.3° in this field of view.

Lattice parameters of the V-doped Sb_2Te_3 sputtered thin film deduced from the FFT patterns were as follows: $a = 0.44 \pm 0.03$ nm and $c = 3.02 \pm 0.02$ nm. These values were calibrated by the lattice constant of the $SrTiO_3$ substrate ($a = 0.3904$ nm).[14] The *a* axis was elongated by 4.2%, whereas the *c* axis was contracted by 0.8% compared with the values of the binary (nondoped) Sb_2Te_3 crystal reported in the literature.[10] The lattice parameter depends on both doping and substrate material, and hence, its variation is not simple.[4,5] The cause of the strain observed in this study is presumed to be due to V addition, but the detailed straining mechanism is unknown.

Figure 3b shows another example of a cross-sectional HREM image showing a grain boundary. In this area, the tilt of the *c* axis from the direction perpendicular to the film surface is 9.4° for the crystal labeled A (left) and 19.7° for the crystal labeled B (right). The interface between crystals A and B is incoherent; interfacial energy is induced to form such a grain boundary. A thin interfacial amorphous layer exists between the Sb_2Te_3 film and the substrate also in this area. The amorphous layer has no obvious roughness, and therefore, the *c* axis tilt as seen in this image is not caused by the roughness or thickness variation of the interfacial amorphous layer.

Plan-View TEM Observation. Figure 4a,b shows the plan-view TEM image and the corresponding SAED pattern of the V-doped Sb_2Te_3 film sputtered for 60 s, respectively. A nanocrystalline structure with a grain size of about 40−80 nm is observed in the TEM image. The grain sizes are consistent with those observed by cross-sectional TEM (Figure 1c). Discontinuous Debye−Scherrer rings indicate the polycrystalline nature of the Sb_2Te_3 film. It should be noted that the 000*l* reflections are missing in the in-plane SAED pattern. This is because the *c* axis preferentially oriented perpendicular to the film plane. Furthermore, reflections with $l \neq 0$ such as $\bar{1}104$ (arrowhead 1), $\bar{1}10\underline{10}$ (arrowhead 2), and $\bar{1}10\underline{13}$ (arrowhead 4) exist. This result corresponds to the *c* axis inclination as observed in Figure 3b. The electron diffraction study unambiguously revealed that there is no in-plane oriented *c* axis in the sputtered V-doped Sb_2Te_3 films. A combination of cross-sectional TEM and in-plane TEM observations revealed the preferential orientation of the *c* axis in the film's normal direction.

Magnetic Properties. Figure 5 shows the temperature dependence of the magnetization of the V-doped Sb_2Te_3 film sputtered for 120 s. Solid and open circles denote the results measured in the film's normal direction and the in-plane direction, respectively. Field cooled (FC) magnetization was measured with an applied magnetic field of 100 Oe. A remarkable hysteresis was observed between the zero-field cooled (ZFC) and the FC magnetization measured perpendicular to the film plane. The ZFC curve shows a maximum at 40 K.

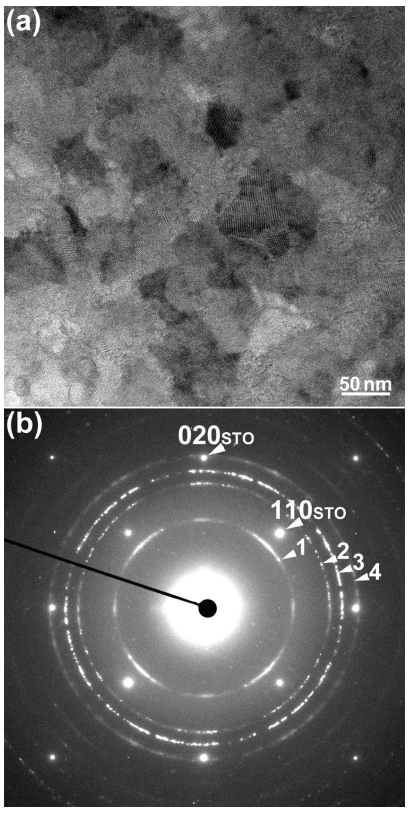

Figure 4. (a) Plan-view TEM image and (b) corresponding SAED pattern of the V-doped Sb_2Te_3 film sputtered for 60 s. Indices of the Debye−Scherrer rings indicated by arrowheads are as follows: 1: $\bar{1}104$, 2: $\bar{1}10\underline{10}$, 3: $\bar{1}2\bar{1}0$, and 4: $\bar{1}10\underline{13}$.

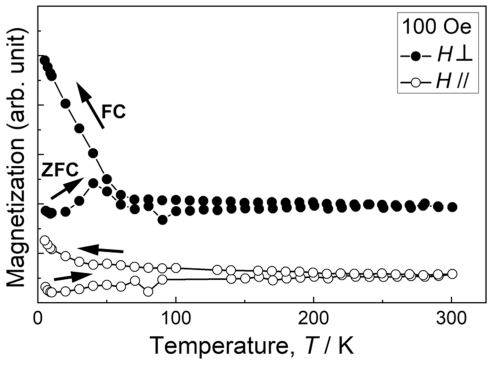

Figure 5. ZFC and FC magnetization curves of the V-doped Sb_2Te_3 film sputtered for 120 s. Solid and open circles denote the results measured in the film's normal direction and the in-plane direction, respectively.

An increase in the FC magnetization was detected at temperatures below 70 K: onset of ferromagnetic order. This result is consistent with the recent study: Chang et al. reported a Curie temperature of ≈70 K for their MBE-grown V-doped Sb_2Te_3 thin films ($Sb_{2-x}V_xTe_3$ with $x = 0.2$).[5] In contrast, the magnetization measurement in the in-plane direction did not show such a remarkable increase in magnetization at low temperatures. This is because the magnetic easy axis of the V-doped Sb_2Te_3 is in the [0001] direction[11] (Figure S1). In the magnetization curves, remanent magnetization and coercivity were both higher in the direction perpendicular to the film plane, whereas the shape of the hysteresis loop showed rather isotropic

https://doi.org/10.1021/acsomega.2c05634
ACS Omega 2022, 7, 40480−40484

behavior (Figure S6). The distribution of *c* axis orientation may contribute to the in-plane magnetization. Saturation magnetization was estimated to be 12 emu/cm^3 at 5 K using a volume of Sb_2Te_3 film estimated from the cross-sectional TEM images. This value corresponds to 2.1 μ_B/V-atom for the $Sb_{38}V_2Te_{60}$. The estimated value is in qualitative agreement with the value deduced from Hund's law for V^{3+} ions (2.8 μ_B). Note that Sb_2Te_3 is a p-type semiconductor with diamagnetic properties.[15,16] Thus, it is considered that V^{3+} ions substituting Sb sites contribute to ferromagnetism at low temperatures.

Elucidation of the V dopant distribution and valence state in the sputtered Sb_2Te_3 film using electron energy-loss spectroscopy is the next step. In the present STEM−EDS analysis (Figures S3 and S4), the doped V appears to be dispersed throughout the Sb_2Te_3 film. Higher resolution elemental analysis including impurities will be necessary in the future.

CONCLUSIONS

In this study, we have fabricated V-doped Sb_2Te_3 thin films ($Sb_{38}V_2Te_{60}$) with an aligned magnetic easy axis using a simple rf-magnetron sputtering method. A combination of cross-sectional and plan-view TEM observations revealed the preferential *c* axis orientation in the film's normal direction. HREM studies revealed the existence of a thin amorphous layer between the Sb_2Te_3 and the $SrTiO_3$ substrate. The amorphous layer relaxes the lattice strain between the sputtered film and the substrate crystal, which would lead to the preferential *c* axis orientation. A remarkable increase in magnetization was detected at temperatures below 70 K in the film's normal direction, which indicates the onset of ferromagnetic order. The origin of the observed ferromagnetism can be attributed to the V^{3+} ions substituting Sb sites.

MATERIALS AND METHODS

Thin films of V-doped Sb_2Te_3 compounds were fabricated by co-deposition of Sb_2Te_3 (99.9%) and V (99.7%) targets via rf-magnetron sputtering onto $SrTiO_3$(001) single crystalline substrates kept at 570 K. The sputtering was performed at 10 mTorr of Ar gas (99.999%) in a chamber having a base pressure of 4×10^{-6} Pa. Sputtering power was set to 30 W in this study. The thickness of the films was controlled by the sputtering duration between 30 and 180 s. Both cross-sectional and plan-view TEM samples were prepared using a tripod polishing technique in combination with low-energy Ar ion milling. The structure and morphology of the prepared specimens were characterized using a JEOL JEM-ARM200F TEM operating at 200 kV equipped with a Schottky field emission gun. All the TEM images and diffraction patterns were recorded using a CMOS camera (Gatan OneView). Compositional analyses were performed using an energy-dispersive X-ray spectrometer (EDS; JEOL JED-2300). V content was determined to be ≈2 at % by TEM−EDS analysis ($Sb_{38}V_2Te_{60}$, see Figure S2) based on the thin film approximation assuming theoretical *k*-factors. Magnetic properties were measured using a superconducting quantum interference device magnetometer (SQUID, Quantum Design, MPMS-XL) in the temperature range between 5 and 300 K with magnetic fields up to 20 kOe.

ASSOCIATED CONTENT

Supporting Information

The Supporting Information is available free of charge at https://pubs.acs.org/doi/10.1021/acsomega.2c05634.

Detailed description of the crystal structure, chemical composition, surface structure, and magnetic properties (PDF)

AUTHOR INFORMATION

Corresponding Author

Kazuhisa Sato − *Research Center for Ultra-High Voltage Electron Microscopy, Osaka University, Ibaraki, Osaka 567-0047, Japan;* orcid.org/0000-0001-9078-2541; Email: sato@uhvem.osaka-u.ac.jp

Complete contact information is available at: https://pubs.acs.org/10.1021/acsomega.2c05634

Author Contributions

Corresponding author conducted the study and wrote the manuscript.

Notes

The author declares no competing financial interest.

ACKNOWLEDGMENTS

The author wishes to thank Mr. K. Kondo, Mr. Y. Fujino, and Mr. T. Yasumura for their help in this study. Magnetic measurements using a SQUID were performed at the low-temperature center (Suita Branch), Osaka University. A part of this study was supported by the Grant-in-Aid for Scientific Research (Grant No. 20K21129 and 21H01764) from the MEXT, Japan. The author thanks Ian McNaught, Ph.D., from Edanz (https://jp.edanz.com/ac) for editing a draft of this manuscript.

REFERENCES

(1) Zhang, H.; Liu, C.-X.; Qi, X.-L.; Dai, X.; Fang, Z.; Zhang, S.-C. Topological insulators in Bi_2Se_3, Bi_2Te_3 and Sb_2Te_3 with a single Dirac cone on the surface. *Nat. Phys.* **2009**, *5*, 438−442.

(2) Jiang, Y.; Wang, Y.; Chen, M.; Li, Z.; Song, C.; He, K.; Wang, L.; Chen, X.; Ma, X.; Xue, Q.-K. Landau quantization and the thickness limit of topological insulator thin films of Sb_2Te_3. *Phys. Rev. Lett.* **2012**, *108*, No. 016401.

(3) Chang, C.-Z.; Zhang, J.; Feng, X.; Shen, J.; Zhang, Z.; Guo, M.; Li, K.; Ou, Y.; Wei, P.; Wang, L.-L.; Ji, Z.-Q.; Feng, Y.; Ji, S.; Chen, X.; Jia, J.; Dai, X.; Fang, Z.; Zhang, S.-C.; He, K.; Wang, Y.; Lu, L.; Ma, X.-C.; Xue, Q.-K. Experimental observation of the quantum anomalous Hall effect in a magnetic topological insulator. *Science* **2013**, *340*, 167−170.

(4) Li, M.; Chang, C.-Z.; Wu, L.; Tao, J.; Zhao, W.; Chan, M. H. W.; Moodera, J. S.; Li, J.; Zhu, Y. Experimental verification of the Van Vleck nature of long-range ferromagnetic order in the vanadium-doped three-dimensional topological insulator Sb_2Te_3. *Phys. Rev. Lett.* **2015**, *114*, No. 146802.

(5) Chang, C.-Z.; Zhao, W.; Kim, D. Y.; Zhang, H.; Assaf, B. A.; Heiman, D.; Zhang, S.-C.; Liu, C.; Chan, M. H. W.; Moodera, J. S. High-precision realization of robust quantum anomalous Hall state in a hard ferromagnetic topological insulator. *Nat. Mater.* **2015**, *14*, 473−477.

(6) Weyrich, C.; Merzenich, T.; Kampmeier, J.; Batov, I. E.; Mussler, G.; Schubert, J.; Grützmacher, D.; Schäpers, T. Magnetoresistance oscillations in MBE-grown Sb_2Te_3 thin films. *Appl. Phys. Lett.* **2017**, *110*, No. 092104.

(7) Momand, J.; Boschker, J. E.; Wang, R.; Calarco, R.; Kooi, B. J. Tailoring the epitaxy of Sb_2Te_3 and GeTe thin films using surface passivation. *CrystEngComm* **2018**, *20*, 340−347.

(8) Kondo, K.; Sato, K.; Yasuda, H. Characterization of Sb_2Te_3/GeTe composite thin films fabricated by rf-magnetron sputtering. *Microscopy* **2019**, *68*, i36.

(9) *Binary Alloy Phase Diagrams*, 2nd ed.; Massalski, T. B., Okamoto, H., Subramanian, P. R., Kacprzak, L., Eds.; ASM International: Materials Park, OH, 1990.
(10) Anderson, T. L.; Krause, H. B. Refinement of the Sb_2Te_3 and Sb_2Te_2Se structures and their relationship to nonstoichiometric $Sb_2Te_{3-y}Se_y$ compounds. *Acta Cryst.* **1974**, *30*, 1307−1310.
(11) Dyck, J. S.; Hájek, P.; Lošťák, P.; Uher, C. Diluted magnetic semiconductors based on $Sb_{2-x}V_xTe_3$ ($0.01 \leq x \leq 0.03$). *Phys. Rev. B* **2002**, *65*, No. 115212.
(12) Zhang, B.; Zhu, W.; Cao, L.; Yu, Y.; Qin, D.; Huang, X.; Deng, Y. Toward reduced interface contact resistance: controllable surface energy of Sb_2Te_3 films via tuning the crystallization and orientation. *ACS Appl. Mater. Interfaces* **2022**, *14*, 10955−10965.
(13) Woo, S.; Jeong, H.; Lee, S. A.; Seo, H.; Lacotte, M.; David, A.; Kim, H. Y.; Prellier, W.; Kim, Y.; Choi, W. S. Surface properties of atomically flat poly-crystalline $SrTiO_3$. *Sci. Rep.* **2015**, *5*, 8822.
(14) Roth, R. S. Classification of perovskite and other ABO_3-type compounds. *J. Res. Natl. Bur. Stand.* **1957**, *58*, 75−88.
(15) Lee, P.-C.; Huang, Y.-C.; Chien, C. H.; Chiu, F. Y.; Chen, Y. Y.; Harutyunyan, S. R. A comparative study of size-dependent magneto-resistance and Hall resistance of Sb_2Te_3 nanoflakes. *Phys. B: Condens. Matter* **2015**, *459*, 12−15.
(16) Harutyunyan, S. R. Thickness-dependent magnetoresistance of Sb_2Te_3 nanoflakes and weak antilocalization effect. *J. Contemp. Phys.* **2015**, *50*, 282−287.

https://doi.org/10.1021/acsomega.2c05634
ACS Omega 2022, 7, 40480−40484